Aswan University Journal of Science and Technology Volume 4, issue 4

Enhancement of Load Frequency Management in Contemporary Hybrid Power Systems Using Renewable Energy Sources

Amira Hassan [a], Mohamed M.Aly [a], Ali Selim [a],
Ahmed Elmelegi [a], Emad A.Mohamed [b]
[a]Department of Electrical Engineering, Faculty of Engineering, Aswan University, Aswan 81542, Egypt
[b]Department of Electrical Engineering, College of Engineering, Prince Sattam Bin Abdulaziz University, Al Kharj 16278, Saudi Arabia

Abstract

Due to climate change, it has become important to shift from conventional generation sources to new renewable energy production. Power systems are becoming more susceptible to issues with low inertia as a result of increased rates of reliance on renewable energy sources (RESs). Fractional order has recently attracted a lot of interest and investigation. As a result, dynamic systems and controllers with fractional order (FO) are becoming more popular. The responsiveness and stability of the load frequency control (LFC) system are enhanced in this article using FO controllers. The performance of the proposed fractional order proportional-integral-derivative (FOPID) controller is compared against the conventional proportional-integral-derivative (PID) controller. The optimal gain values of the two controllers will be optimized utilizing the marine predator optimization algorithm (MPA), and a performance comparison was carried out with several objective functions. After comparing the settling times, overshoot, undershoot, oscillation of frequency deviation, and tie-line power of the single and dual-area hybrid power systems (SAHPS & DAHPS), it is possible to conclude that, in the occurrence of load disturbance changes and the widespread use of RESs, the suggested FOPID controller performs more effectively and is more robust than the conventional controller. It minimized the ISE after 32 iteration with 83.73%, IAE with 75%, ITSE with 93.77%, and ITAE with 83.58% compare to the PID controller at load variation.

Keywords: Fractional order (FO), Marine Predators Algorithm (MPA), Renewable energy sources

Corresponding author E-mail: eng_ahelmelegi2@yahoo.com

Received September 21, 2024, received in revised form, October 6, 2024, accepted October 9, 2024.

(ASWJST 2021/ printed ISSN: 2735-3087 and on-line ISSN: 2735-3095) https://journals.aswu.edu.eg/stjournal

Nomenclature

Δf_1	Frequency deviation of the area 1
Δf_2	Frequency deviation of the area 2
D_i	Damping factor of two area
H_i	Inertia constant of two area
R_i	Droop constant of two area
B_i	Frequency bias value of two area
$\Delta P_H, \Delta P_{Rth}, \Delta P_{PV}, \Delta P_W$	Power generations of hydro, thermal, PV and wind plant
ΔP_{tie}	Tie-line power flow between the two-area
T_{gh}	Speed governor time constant of hydro turbine
T_{rh}	Transient droop time constant of hydro turbine speed governor
T_{rs}	Speed governor reset time of the hydro turbine
T_W	Nominal string time of water in penstock
T_r	Time constant of reheater steam turbine
T_{sg}	Governor time constant of thermal plan
K_r	Gain of reheater steam turbine
T_{WT}, T_{PV}	Time constant of wind and PV
K_{WT}, K_{PV}	Gain of wind and PV
K_P, K_i, K_d	Proportional, integral and differential gains for PID controller
LFC	load frequency control
MPA	Marine Predator Algorithm
λ , μ	*Fractional order of integration and differentiation operator*
IAE	Integral-absolute error
ISE	Integral-squared error
ITAE	Integral-time absolute error
ITSE	Integral time-squared error

1. Introduction

1.1. Overview

The world's governments have set high goals for the replacement of conventional fossil fuel sources with renewable energy sources (RESs) as a result of climate change [1]. In recent years, enormous wind

and solar (PV) power plants have been put into operation [2]. However, RESs have a weak inertial response because of their structural design that is dependent on power electronics. Power networks are susceptible to frequency fluctuations because renewable energy sources (RESs) are intermittent. These fluctuations can have severe consequences, such as a complete or partial power system shutdown [3]. Furthermore, variations in the required load and the generation power mismatches between loading and generation cause fluctuation of frequency and variations in tie power from their specified parameters. As a result, load frequency control (LFC) has emerged as a critical component for ensuring the reliable and secure operation of electrical networks [4]. The LFC is vital for ensuring the equilibrium of both isolated and linked power systems during fluctuations in load and RESs variations. In power systems, frequency regulation often involves two distinct control loops. The first loop is modeled by the principal control loop, which controls the speed governor. However, the power system's changes cannot be contained or overcome by the primary control loop. The secondary control loop, on which the second loop is built, primarily aids in managing frequency changes and fluctuations in linked power throughout the various electrical network zones [5, 6].

1.2. Literature Review

The PID controller is well-known and often utilized. Due to their ease of implementation, ease of parameter adjustment, and widespread use in power system control applications. This controller is frequently employed to lessen steady-state error, boost stability, and attenuate system oscillations [7, 8]. Since the power of the integral or derivative in these controllers is one, these controllers are of integer order (IO). LFC systems primarily employ straightforward PI controllers and I controllers, whose parameters are typically set using conventional control theory or attempt and error methods. Although the I controller has zero stable-state frequency variation, its dynamic performance is weak. In a linked network electric system, the fundamental approaches to controller design are ineffective for achieving high dynamic flexibility under various load change situations and disruptions. Many methods, including robust control, have been presented by authors to support system frequency stability [9, 10, 11]. Variable architecture control [12, 13], and optimizing a proportional-integral-derivative (PID) controller using several techniques [14, 15, 16]. In [15], the authors determined the PID controller's ideal gains for enhancing the system's frequency using a genetic algorithm (GA). The two-degree-of-freedom (2DOF)-PID controller's parameters were optimized in [17] using teaching-learning optimization. In [18], to determine the ideal PID controller values, the bacterial foraging optimizer (BFO) was used. To determine the PID controllers' ideal settings, numerous methods were employed, such as the grey wolf optimizer (GWO) [19], Jaya approach [20], equilibrium optimization algorithm (EOA) [21], and the linear-quadratic-Gaussian technique [22]. Several control theories have been employed to determine the values of LFC in connected electrical networks. PID controller values have been developed in [23] using the stability boundary locus (SBL) technique. Additionally, it has been applied in [24] to improve the LFC of the micro grid at different communication time delays. Moreover, PI values are optimized via Harris Hawks optimization (HHO) in [25]. These controllers are straightforward fixes, but they are unable to completely reduce the disturbances in the electrical network system. Fractional order control has

become a very effective algorithm for systems operating in unpredictable environments in recent years.

1.3. Contributions

The contributions made in the current article can be summed up as follows:

- A proposal for FOPID is introduced in this article for LFC in SAHPS & DAHPS, with the controller equipped in every region for reducing the frequency and interchange power variations.
- In this proposal, five parameters must be improved to attain the best FOPID performance, and an optimization technique called MPA is utilized to obtain the ideal gains of the suggested controller settings.
- The efficacy, robustness, and dominance of the proposed FOPID-based MPA over the traditional PID are examined in relation to load disturbances, parameter uncertainties, and strong penetration of RESs effects.

2. Mathematical Model Representation

Load frequency regulation in power systems has been a significant problem during disturbances in load demand and reliance on RESs. In this section, various PS models are constructed and studied to assess the performance of the study proposal. Among those are SAHPS and DAHPS, in each of the two cases of study incorporating the effect of RESs. In the event of unfavorable circumstances, like changes in parameters and load uncertainties, the control unit monitors the system frequency and tied power perversion and attempts to return the system to its normal operating state. Fig. 1 and Fig. 2 depict the schematic models of SAHPS and DAHPS, respectively, for the proposed system. The theoretical values for the suggested system SAHPS & DAHPS are listed in Appendix A [26,27,28] at the bottom of the paper.

2.1. MODELLING OF SAHPS

The tested SAHPS is composed of a reheat thermal generation, a hydropower generation, and RESs consisting of a photovoltaic PV solar plant and a wind plant. The transfer function of individual blocks in each power plant unit is explained as follows:

Thermal Plant

$$G_{th_R}(s) = \frac{sK_rT_r + 1}{sT_r + 1} \quad (1)$$

$$G_{th_G}(s) = \frac{1}{sT_i + 1} \quad (2)$$

where, $G_{th_R}(s)$ refers to governor turbine, and $G_{th_G}(s)$ refers to reheat turbine of the thermal power plant

Hydraulic Plant

$$G_{hy_G}(s) = \frac{1}{sT_{gh}+1} \quad (3)$$

$$G_{hy_D}(s) = \frac{sT_{rs}+1}{sT_{rh}+1} \quad (4)$$

$$G_{hy_P}(s) = \frac{-sT_w+1}{0.5sT_w+1} \quad (5)$$

where, $G_{hy_G}(s)$ refers to governor turbine, $G_{hy_D}(s)$ refers to drop compensation, and $G_{hy_P}(s)$ refers to penstock turbine of the hydro power plant.

PV solar plant

Temperature and sunshine intensity determine how much electricity may be generated from photovoltaic cells at any one time [29,30]. The first-order transfer function of PV is given below [31] :

$$G_{PV}(s) = \frac{K_{PV}}{T_{PV}s+1} \quad (6)$$

where, K_{PV} denote the PV gain, while T_{PV} denote PV time constant.

Wind plant

The mechanical power production of a wind turbine (WT) system is highly variable because wind speed is intermittent. The WT dynamic response model can be demonstrated using a first-order transfer function, as seen in [32]:

$$G_{WT}(s) = \frac{K_{WT}}{T_{WT}s+1} \quad (7)$$

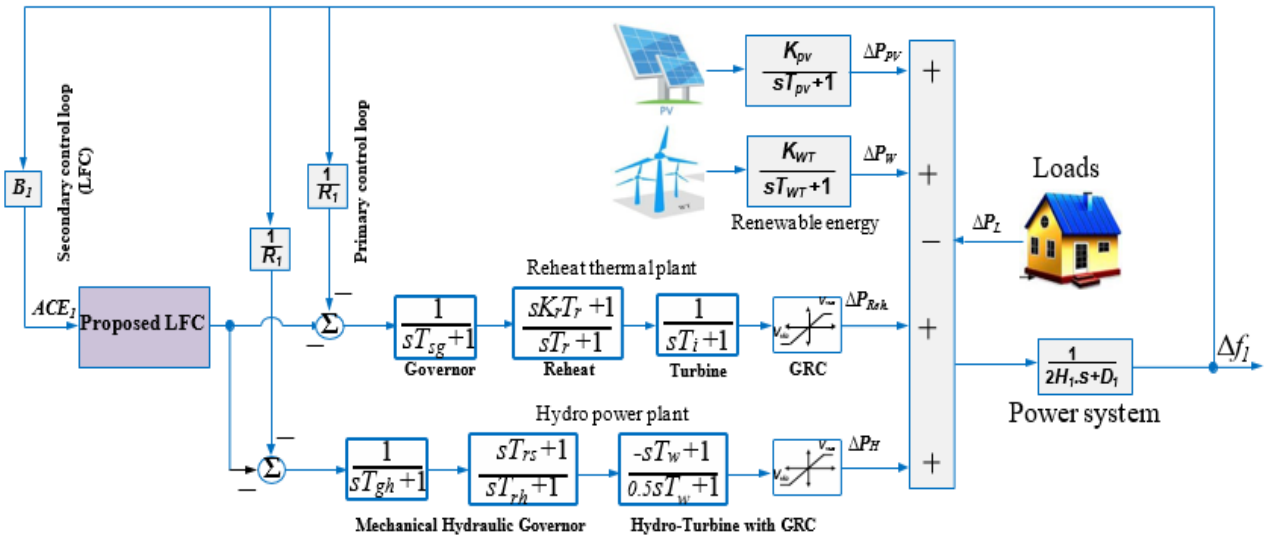

Figure 1: Model of studied SAHPS [28].

2.2. MODELLING OF DAHPS

The LFC model on which the test has been executed is a DAHPS. The model includes a thermal and a hydro generation with RESs for each area. Through a tie line that connects the dual areas, electricity can flow between the connected areas. For a dual area system, the area control error for region 1 (ACE_1) and region 2 (ACE_2) is given by

$$ACE_1 = \Delta P_{tie,1} + B_1\ \Delta f_1 \tag{8}$$

$$ACE_2 = -\Delta P_{tie,2} + B_1\ \Delta f_2 \tag{9}$$

where, $\Delta P_{tie,1}$, and $\Delta P_{tie,2}$ are the tie-line for region 1 and region 2, respectively. while (B_1), and (B_2) are the frequency bias coefficient for region 1 and region 2, respectively.(B_1), and (B_2) are given by

$$B_1 = D_1\ + \frac{1}{R_1} \tag{10}$$

$$B_2 = D_2\ + \frac{1}{R_2} \tag{11}$$

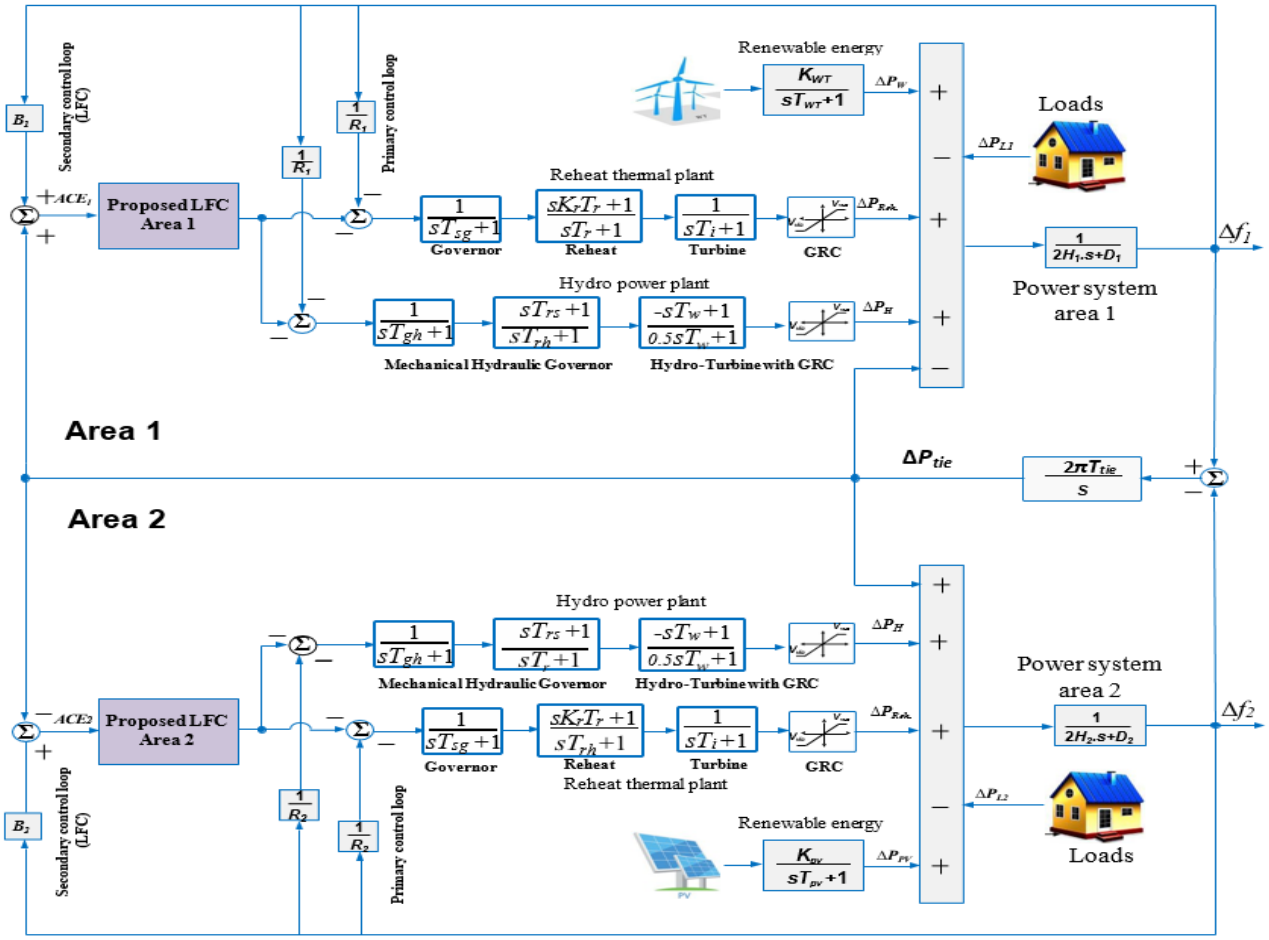

Figure 2: Model of studied DAHPS [28].

2.3. Proposed FOPID Controller

Many power system research proposals use integer control methods for linear frequency control (LFC) in the literature. The PID has been utilized extensively in the literature to address problems with frequency stability. The PID structure's transfer function is shown as follows [27,28]:

$$C(S) = \frac{Y(S)}{R(S)}$$

$$= K_{\mathrm{p}} + \frac{K_i}{S} + K_{\mathrm{d}} S \qquad (12)$$

where the principal gains for the integral, proportional, and derivative components are, respectively, K_i, K_p, and K_d. Furthermore, the unique fractional order FO/PID structure is obtained by combining the advantages of the PID scheme and the FO calculus. The transfer function mentioned below can be used to represent this FO/PID controller [27,28]:

$$\mathrm{C(S)} = \frac{Y(S)}{R(S)} = K_{\mathrm{p}} + \frac{K_i}{S^{\lambda}} + K_{\mathrm{d}} S^{\mu} \tag{13}$$

where, λ and μ denote to the exponential terms for the integral, and derivative factors, respectively.

3. Objective Function and Tunning Process

In this paper, the ideal gains in the suggested and conventional controllers are found using the MPA. The optimization process's function must keep the frequency deviations' minimal values constant in case of a single area (Δf_1), while in case of a dual area (Δf_1) of region 1 and (Δf_2) in region 2 additionally to reduced parameters of the tied power (ΔP_{tie}).The proposed optimization procedure employs the integral-squared error (ISE), integral time-squared error (ITSE), integral absolute error (IAE), and integral time absolute error (ITAE), four commonly used techniques for estimating errors. Based on the intended constraints and requirements, the effectiveness and supremacy of the suggested controller and the conventional controller are evaluated using the four techniques. They are shown as follows: For DAHPS: -

$$ISE = \int_0^{t_s} \left((\Delta f_1)^2 + (\Delta f_2)^2 + (\Delta P_{tie})^2 \right) dt \tag{14}$$

$$ITSE = \int_0^{t_s} \left((\Delta f_1)^2 + (\Delta f_2)^2 + (\Delta P_{tie})^2 \right) t.dt \tag{15}$$

$$IAE = \int_0^{t_s} \left(abs(\Delta f_1) + \mathrm{abs}(\Delta f_2) + abs(\Delta P_{tie}) \right) dt \tag{16}$$

$$ITAE = \int_0^{t_s} \left(abs(\Delta f_1) + abs(\Delta f_2) + abs(\Delta P_{tie}) \right) t.dt \tag{17}$$

The results of the restricted evaluation of the efficiency indicator are the optimal values for PID controller gains. The controller gains' lower and upper bounds are the limitations. The following is an expression of the optimization issue:

$$\begin{gathered} K_P^{min} \le K_P \le K_P^{max} \\ K_i^{min} \le K_i \le K_i^{max} \\ K_d^{min} \le K_d \le K_d^{max} \end{gathered} \tag{18}$$

The optimal values for FOPID controller gains. The following is an expression of the optimization issue:

$$\begin{gathered} K_P^{min} \le K_{P1}, K_{P2}P \le K_P^{max} \\ K_i^{min} \le K_{i1}, K_{i2}P \le K_i^{max} \\ K_d^{min} \le K_{d1}, K_{d2} \le K_d^{max} \\ \lambda^{min} \le \lambda_1, \lambda_2 \le \lambda^{max} \\ \mu^{min} \le \mu_1, \mu_2 \le \mu^{max} \end{gathered} \tag{19}$$

Where the limitations for various adjusted controllers are contained within the specified upper bounds as *max* and lower parameters of control gains as *min*. The smallest parameters of control gains (K_i^{min}, and K_d^{min}) are at zero values, and their maximum

(K_i^{max}, and K_P^{max}) values are adjusted at 5. Whereas (λ^{min}, and μ^{min}) are set at zeros, and (λ^{max}, and μ^{max}) are utilized at the value of 1. For SAHPS and DAHPS cases, Tables 1 and 2 list the optimal gain parameters of the proposed FOPID and PID controller utilizing the MPA technique. Additionally,Table 3 shows the objective function values through the use of the two different controllers, PID and FOPID, in the cases of ISE, IAE, ITSE, and ITAE.

Table 1: Gains values of two controllers for SAHPS by using MPA

Controller	Coefficients				
	K_p	K_i	K_d	λ	μ
Proposed FOPID	1.5615	1.8463	0.9990	0.9594	0.8990
PID	0.3884	0.4238	0.6095	-	-

Table 2: Gains values of two controllers for DAHPS by using MPA

Controller	Area	Coefficients				
		K_p	K_i	K_d	λ	μ
Proposed FOPID	Area 1	1.6311	1.994	1.1731	0.8854	0.8852
	Area 2	1.082	0.98453	1.9281	0.8714	0.9429
PID	Area 1	1.9245	1.0567	1.6126	-	-
	Area 2	1.7905	0.8053	1.1428	-	-

3.1. The Principle Operation of Marine Predator Algorithm (MPA)

The freshly built MPA optimizer serves as the foundation for the suggested design procedure. The MPA is applied to ideal establish the different variables of the FOPID and PID controllers. The MPA is a contemporary method inspired by the efficient movements of marine predators while they search for prey. One wonderful feature of MPA is that both predators and prey are regarded as search members [33]. The common methods for determining the predator's movement strategy are Levy and Brownian based movements [33]. The prey-to-predator speed ratio is a crucial factor in the MPA algorithm, transitioning the optimization process between phases. The primary steps in the MPA workflow, which is displayed in Fig. 3, are as follows:

1) Initialization process: Two models of mathematics are built: the Elite and the Prey. The Prey model uses variable random places that are uniformly dispersed over the proposed area. Meanwhile, the placement vector with the preferable fitness function is iterated by Elite mathematical modeling.

2) Phase no.1 (the first one-third of the repetitions): In this instance, the predator remains still while the prey moves utilizing the Brownian method. Wherein, the prey use equations to update their positions according to the following relations (20) and (21) [33]:

$$S_{\mathrm{i}} = R_{\mathrm{B}} \times (Elite_{\mathrm{i}} - R_{\mathrm{B}} \times Z_{\mathrm{i}}), i = 1,2, \dots, n \quad (20)$$

$$Z_{\mathrm{i}} = Z_{\mathrm{i}} + 0.5R \times S_{\mathrm{i}} \quad (21)$$

where S_i represents step size, whereas R_B symbolizes the Brownian motion vector, and R is random number vector among [0,1].

3) Phase no.2 (the second one third of repetitions): Wherein the prey uses Levy's motion and the predator utilizes Brown's motion. Two subsections, the first of which uses (22) and the second of which uses (23), depict the population at this point. On the other hand, the following positions are updated in the second subsection using (24) and (25): In [34], the MPA's concepts and its operation are presented using mathematical models:

$$S_{\mathrm{i}} = R_{\mathrm{L}} \times (Elite_{\mathrm{i}} - R_{\mathrm{L}} \times Z_{\mathrm{i}}), i = 1,2,\ldots,n/2 \quad (22)$$

$$Z_{\mathrm{i}} = Z_{\mathrm{i}} + 0.5R \times S_{\mathrm{i}} \quad (23)$$

where, R_L is the indiscriminate value according to Lévy's motion distribution.

$$S_{\mathrm{i}} = R_{\mathrm{B}} \times (R_{\mathrm{B}} \times Elite_{\mathrm{i}} - Z_{\mathrm{i}}), i = 1,2,\ldots,n/2 \quad (24)$$

$$Z_{\mathrm{i}} = Elite_{\mathrm{i}} + 0.5CF \times S_{\mathrm{i}} \quad (25)$$

where,

$$CF = \left(1 - \frac{t}{t_{\max}}\right)^{2\frac{t}{t_{\max}}} \quad (26)$$

where, CF is step size of predator, whereas t and $t_{\max}$ are the current and maximum values for repetitions.

4) Phase no.3 (last one-third of the repetitions): in this stage, Levy's motion is used by the Predator, and (27) and (28) [29] are used to update the Prey.

$$S_{\mathrm{i}} = R_{\mathrm{L}} \times (R_{\mathrm{L}} \times Elite_{\mathrm{i}} - Z_{\mathrm{i}}), i = 1,2,\ldots,n \quad (27)$$

$$Z_{\mathrm{i}} = Elite_{\mathrm{i}} + 0.5CF \times S_{\mathrm{i}} \quad (28)$$

5) Finishing process: At the end of each repetition, the preferable position is retained in the Elite model, which presents the preferable position at the conclusion of each repetition.

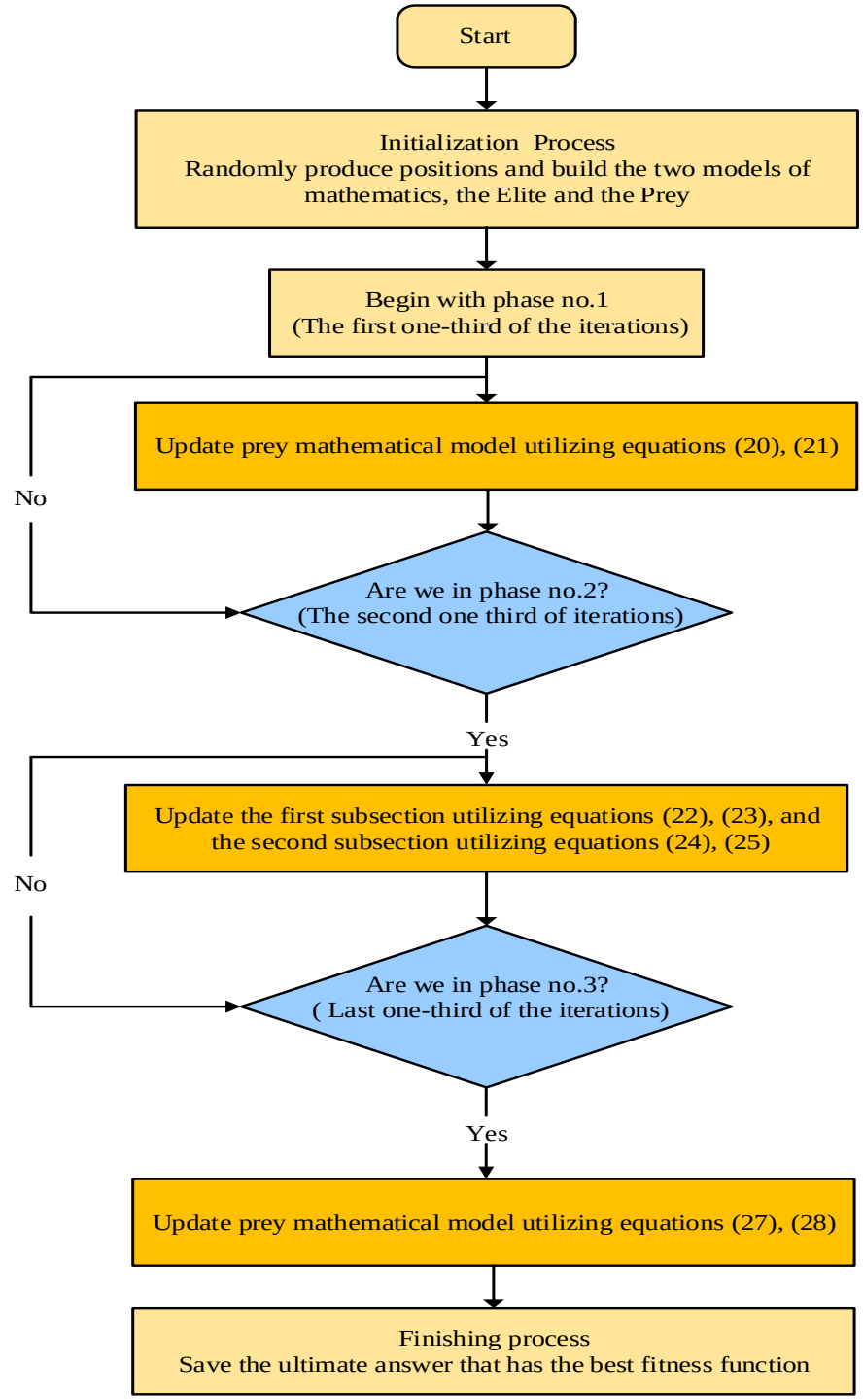

Figure 3: Flowchart for MPA

4. Examination of the simulation's outcomes

Using the chosen SAHPS & DAHPS models, the functionality of the proposed controller-based MPA is examined and assessed while taking various operational scenarios for RESs penetrations and load changes into account. In this study, to assess the scenarios, MATLAB/SIMULINK software is utilized. The MPA is created as a (.m file) and then interacted with the evaluated SAHPS and DAHPS models' SIMULINK

structure to run optimization procedures. Furthermore, the results of the simulation of the suggested controller are contrasted with those of the PID controller to validate its supremacy with regard to overshooting, undershooting, and settling time for variations in frequency, as well as linked power variability according to various cases of fluctuations in the various scenarios. To validate a proposed controller, six cases of study have been presented against load fluctuation, variations in frequency, as well as linked power variability as follows:

4.1. Cases of SAHPS

Case 1

The first case tested the proposed control system performance against 10% stepping load change at the beginning time of the simulation. The frequency deviation is depicted in Fig. 4. The figure shows that the suggested controller offers a lower frequency deviation value than the classical PID controller. Moreover, Fig. 4 proves demonstrates the improved performance of the suggested controller at the instant of disturbance with a small settling time and minimal overshoot/undershoot contrast to PID controllers as listed in Table 4.

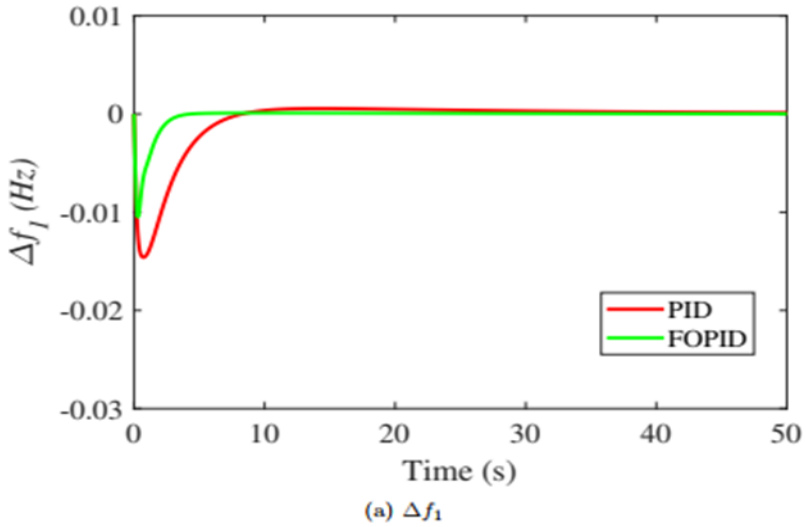

Figure 4: The system's dynamic response in case 1.

Case 2

The power system in this instance is examined in relation to a 10% step load change at the start of the simulation as well as the penetration of wind and photovoltaic power plants. As seen in Fig. 5, the integration of PV and wind power plants is connected in the system at 20 s. The response of frequency variation is shown in Fig. 6. The proposed MPA-optimized FOPID controller has successfully regulated the frequency response under the effects of the penetration of PV and wind

generation plants, as shown in Fig. 6. Also, as shown in Table 3 and Table 4, the FOPID controller outperformed the previous control method by dampening overall system perversions and obtaining the lowest objective function minimization through the use of the MPA technique in the cases of ISE, IAE, ITSE, as well as ITAE to acceptable levels.

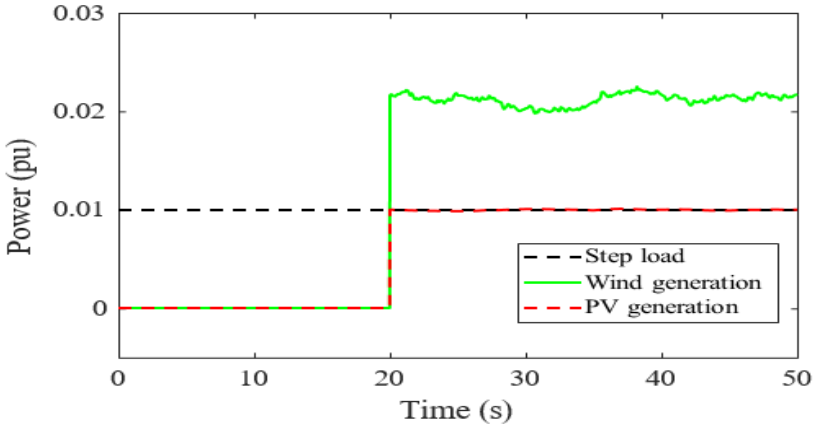

Figure 5: Load and RESs profiles for case 2.

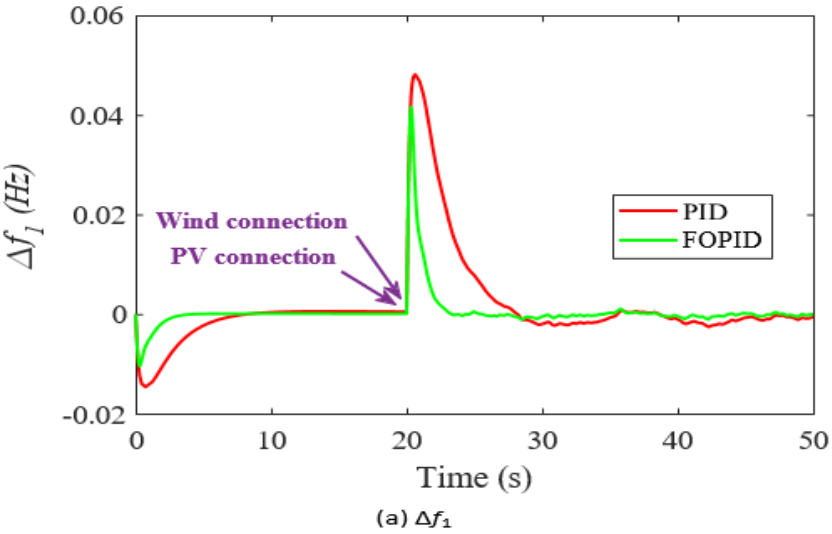

Figure 6: The system's dynamic response in case 2

Table 3: Performance assessment standards for the several case studies

Scenario	Controller technique	performace indices			
		ISE	IAE	ITSE	ITAE
Case 1	PID	4.3641e-04	0.0576	7.6825e-04	0.4295
	FOPID	7.0986e-05	0.0144	4.7843e-05	0.0705
Case 2	PID	0.0049	0.2166	0.0979	4.2770
	FOPID	9.5738e-04	0.0583	0.0183	1.0985
Case 3	PID	5.1390e-04	0.1429	0.0317	9.5484
	FOPID	9.8901e-05	0.0354	0.0060	2.2710
Case 4	PID	0.2766	2.9889	46.7475	447.3277
	FOPID	0.2254	2.6529	35.1482	378.5511
Case 5	PID	0.0016	0.2745	0.1052	17.8000
	FOPID	2.9961e-04	0.0789	0.0198	5.2699
Case 6	PID	0.0025	0.3138	0.1485	19.4238
	FOPID	0.0018	0.3116	0.0878	18.4503

Table 4: Response parameters for the several case studies

Scenario	Controller	Δf_a			Δf_b			ΔP_{tie}		
		MO	MU	ST	MO	MU	ST	MO	MU	ST
Case 1 at zero s	PID	0.00055	0.01453	29.02	-	-	-	-	-	-
	FOPID	-	0.01006	8.76	-	-	-	-	-	-
Case 2 at 20 s	PID	0.04751	0.002169	47.55	-	-	-	-	-	-
	FOPID	0.04074	0.0004122	34	-	-	-	-	-	-
Case 3 at 20 s	PID	0.0002742	0.01142	60.92	0.0002807	0.007242	72.52	0.0001508	0.00262	78.6
	FOPID	-	0.009452	40.06	-	0.004516	43.16	-	0.001476	45.66
Case 4 at 210 s	PID	osci	osci	260.7	osci	osci	275.9	osci	osci	285.1
	FOPID	0.3348	-	232	0.2312	-	231.3	0.07852	-	256.5
Case 5 at 50 s	PID	-	0.007457	73.56	-	0.01156	72.76	0.002703	-	79.64
	FOPID	-	0.004319	61.72	-	0.009479	57.14	0.001525	-	66.12
Case 6 at 80 s	PID	0.02067	0.001004	116.8	0.021	0.000591	117.9	0.005387	0.0004008	115.4
	FOPID	0.01559	-	103.5	0.011	-	105.7	0.002567	-	105.7

4.2. Cases of DAHPS

Case 3

According to Fig. 7, in this instance, the interconnected two-area electrical network experiences two stepping-load disturbances, with 1% in region 1 and 1% in region 2 at times t = 20s and 100s, respectively. The suggested LFC-based using the enhanced controller is contrasted with classical PID controllers in order to confirm its robustness. The frequency deviation and tied power response of the suggested system with the effect of the stepping load variations are illustrated in Fig. 8. It is evident that, when compared to PID control, the FOPID controller performs more steadily and quickly in correcting frequency of the system and linked power aberrations.

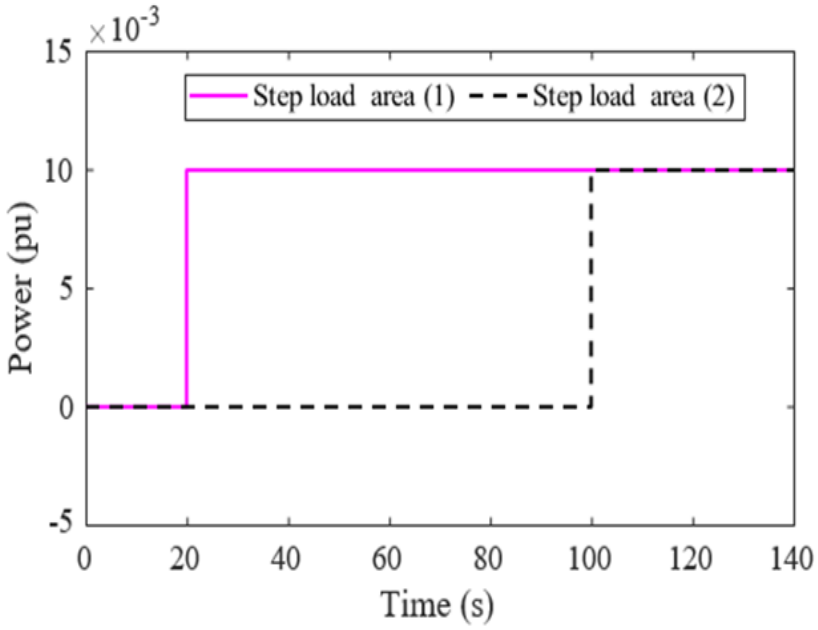

Figure 7: Load profiles for case 3.

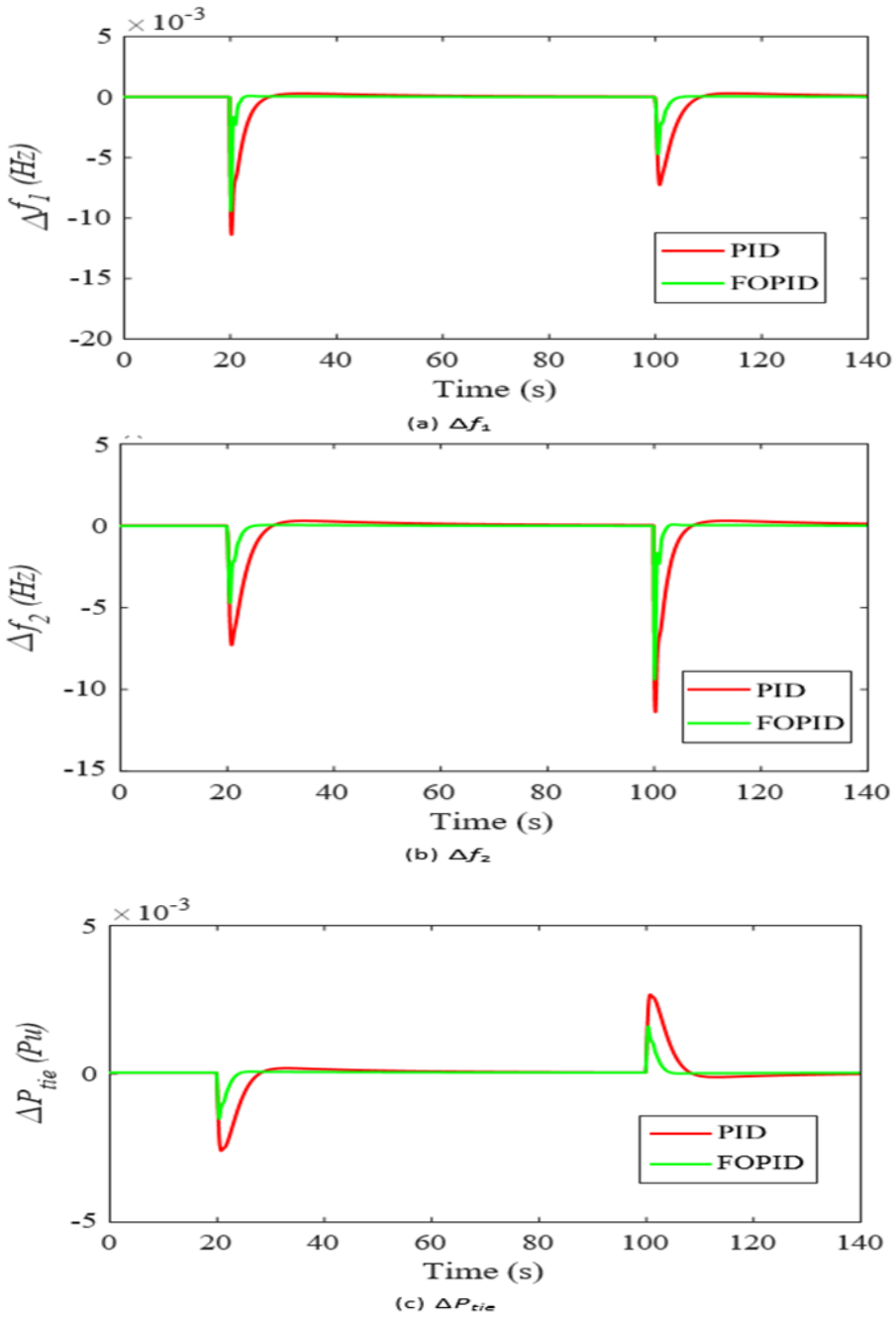

Figure 8: System dynamic response at case 3

Case 4

To confirm the sturdiness of the suggested FOPID controller, the electrical network in this instance is tested during applied and removed load penetration in region 1 at 30 sec, 120 sec, and 210 sec, as indicated in Fig. 9a. The suggested controller can considerably increase the system's stability of the frequency and the linked power deviation across

the dual area to less values than the traditional PID controller, as shown by Figs. 9b, Fig. 9c, and Fig. 9d.

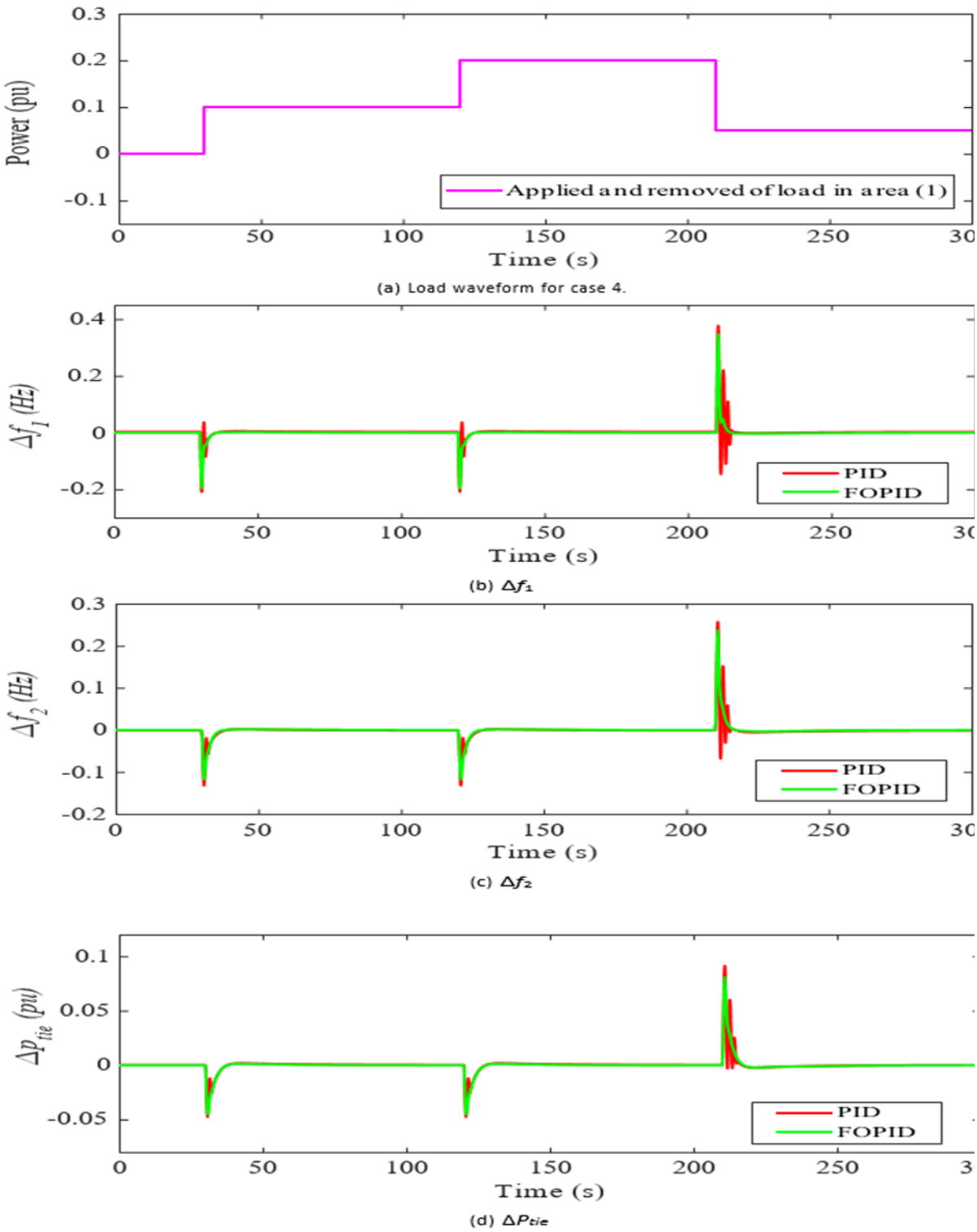

Figure 9: System dynamic response at case 4.

Case 5: RESs disorders

In this case, the proposed system utilizing the MPA-based improved FOPID controller is examined according to extreme conditions of loading and RESs fluctuations. Here, the PV generation is connected to the tested system at period = 20s at area 2, the wind plant unit is connected at time = 80s at area 1, and a variation step-load of 1% at period = 50s at area 2 is connected as illustrated in Fig. 10a. It is evident from Fig. 10 that the proposed FOPID controller was successful in reducing the frequency variations in regions 1 and 2 to (Δf_1=0.004319 Δf_2, =0.009479), while quickly settling time in areas 1 and 2 to values (61.72, 57.14) compared to values (Δf_1=0.007457, Δf_2=0.01156) and values (73.56, 72.76) of PID controller. Thus, an improvement of (42.1, 18) % in frequency deviations and (16.1, 21.5) % in settling time is observed. The advantages of the FO integral are shown in this case, and the derivative indicates that the suggested controller can improve frequency deviations and settling time.

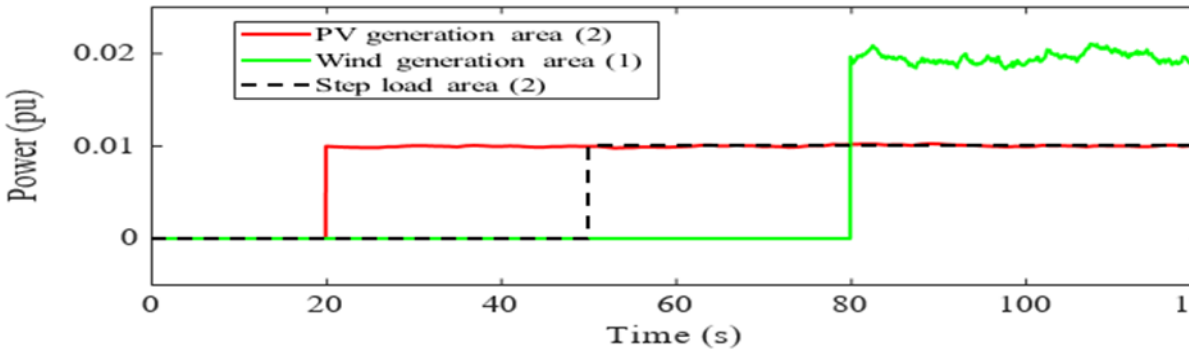

(a) The patterns of wave for power plants and load in case 5.

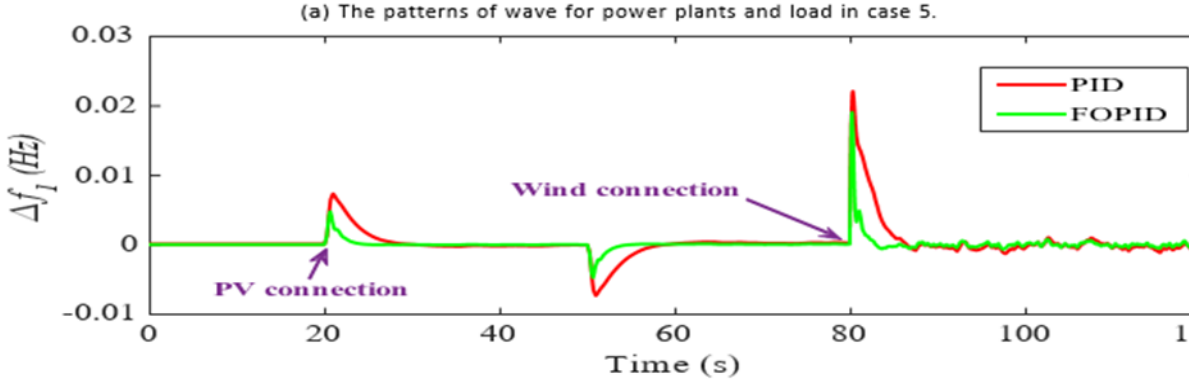

(b) Δf_1

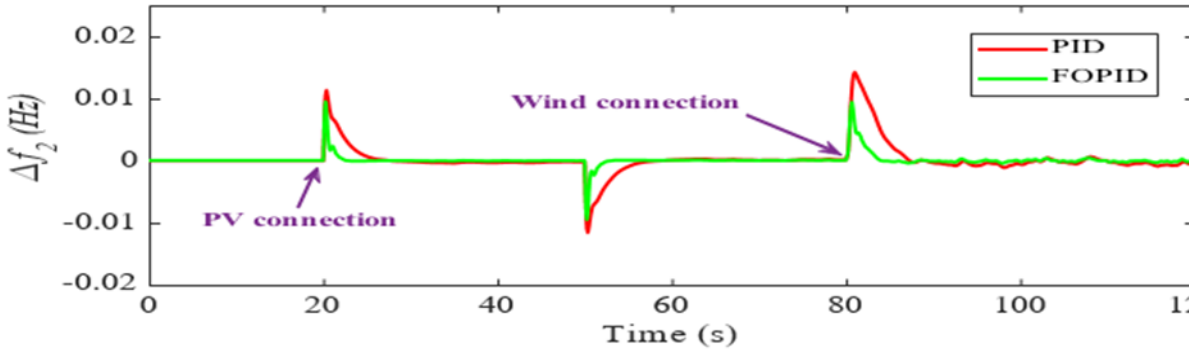

(c) Δf_2

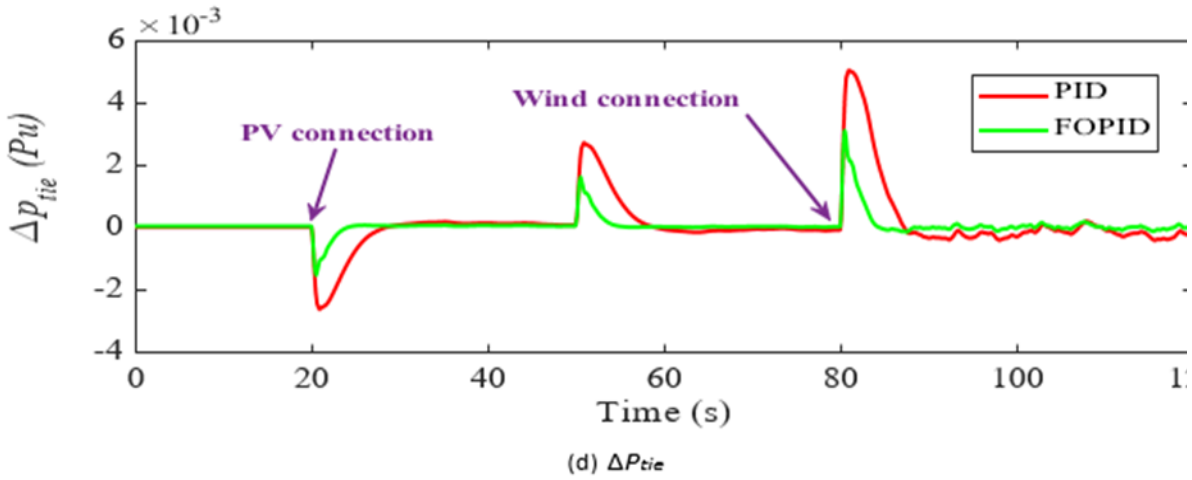

(d) ΔP_{tie}

Figure 10: System dynamic response at case 5.

Case 6: RESs disorders and system uncertainties.

The endurance of the suggested FOPID controller is analyzed for the interrelated electrical system with instabilities in the system parameters. The power network under test is subjected to identical conditions as in instance 5, with a 45% decrease in system inertia and a corresponding percentage variation in other system metrics. This case has the purpose of validating the integrity of an electrical network system under various unpredictable scenarios. The dynamic responses of the system under study are depicted in Fig. 11 with respect to the frequency and linked power changes. It can be mentioned that the suggested FOPID controller outperformed the others in terms of linked power control and frequency limitations.

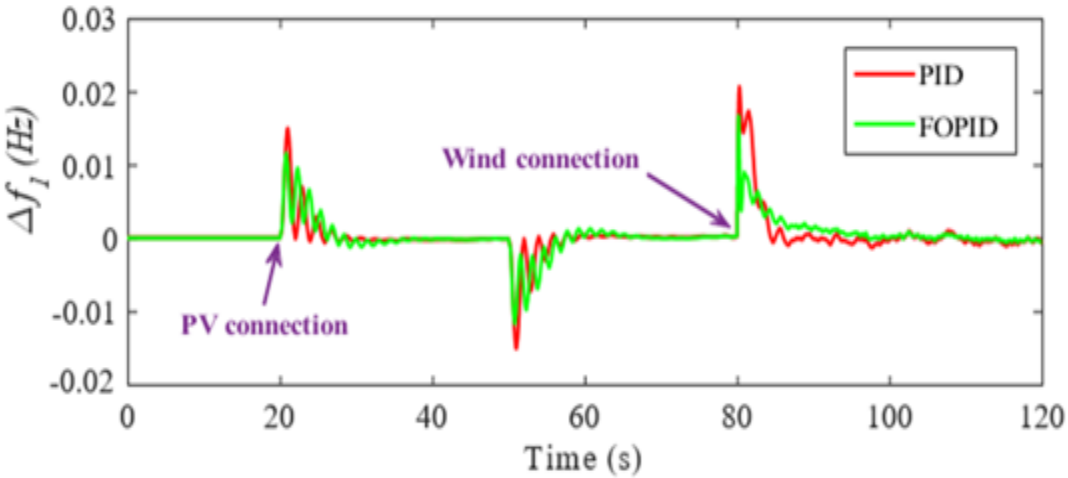

(a) Δf_1

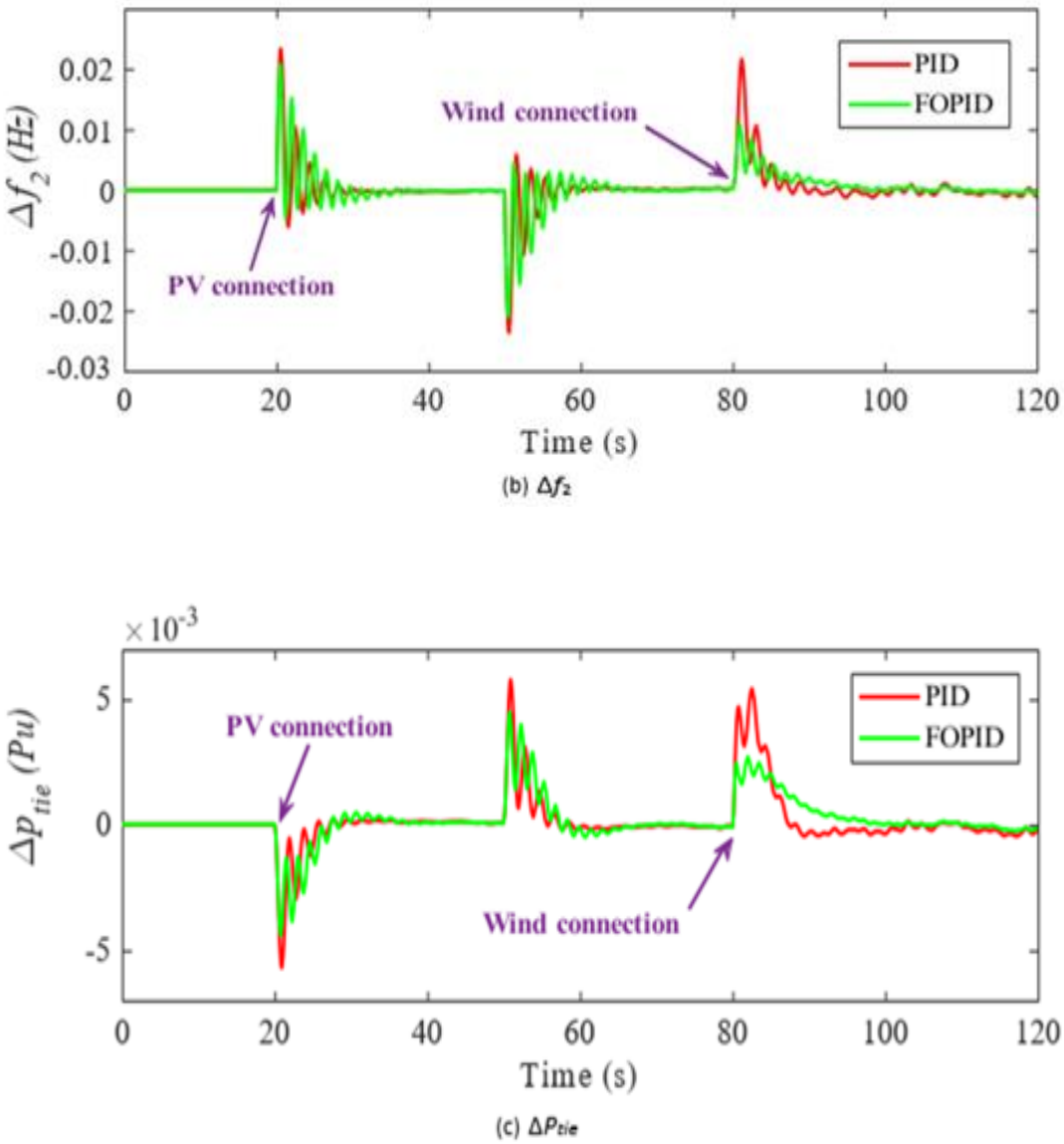

Figure 11: System dynamic response at case 6.

5. Conclusions

In this manuscript, the frequency regulation of the suggested single and dual-area hybrid electrical network system SAHPS & DAHPS has been examined using the classical PID and the proposed FOPID-based MPA technique under the influence of load change and renewable energy sources (RESs) fluctuations. Whereas, six different scenarios are applied to prove how well the performance of the suggested control strategy. The proposed FOPID controller employ MPA method to solve the LFC issue in the two tested SAHPS & DAHPS systems through a variety of cases, including applying different load variations like (step load and multiply load changes) and penetrating RESs. The simulation findings in this manuscript guarantee the reliability of the suggested FOPID controller-based MPA contrasted to the PID controller-based MPA in improving both

tested systems' dynamic response characteristics in terms of settling times, undershoots, overshoots, and reduce values for performance indices of the objective function (ISE, ITSE, IAE, and ITAE) in various examined cases. For example, it is observed that the proposed technique was successful in reducing the frequency variations in regions 1 and 2 of the DAHPS to 42.1%, and 18 % in frequency deviations beside 16.1%, and 21.5 % in settling time values.

Appendix A

Power system's basic parameters with ($i \in \{1,2\}$):-

R_i= 2.4 Hz/MW, B_i= 0.425 MW/Hz, T_{sg}= 0.08 s, T_i= 0.3 s, K_r= 0.5, T_r= 10 s, T_{gh}= 48.75 s, T_{rh}= 0.513 s, T_{rs}= 5 s, T_w= 0.3 s, H_i= 0.0833 p.u.s, D_i= 0.00833 P.U/Hz, T_{tie}= 0.086, , T_{PV}= 1.3 s, K_{PV}= 1, T_{WT}= 1.5 s, K_{WT}= 1

References

[1] S. M. Said, M. Aly, B. Hartmann, A. G. Alharbi, E. M. Ahmed, SMES-based fuzzy logic approach for enhancing the reliability of microgrids equipped with PV generators, IEEE Access 7 (2019) 92059–92069. doi:10.1109/access.2019.2927902.

[2] S. M. Said, M. Aly, H. Balint, An efficient reactive power dispatch method for hybrid photovoltaic and superconducting magnetic energy storage inverters in utility grids, IEEE Access 8 (2020) 183708–183721. doi:10.1109/access.2020.3029326.

[3] E. A. Mohamed, E. M. Ahmed, A. Elmelegi, M. Aly, O. Elbaksawi, A.-A. A. Mohamed, An optimized hybrid fractional order controller for frequency regulation in multi-area power systems, IEEE Access 8 (2020) 213899–213915. URL: https://doi.org/10.1109/access.2020.3040620. doi:10.1109/access.2020.3040620.

[4] A. Latif, S. S. Hussain, D. C. Das, T. S. Ustun, A. Iqbal, A review on fractional order (FO) controllers' optimization for load frequency stabilization in power networks, Energy Reports 7 (2021) 4009–4021. doi:10.1016/j.egyr.2021.06.088.

[5] S. Oshnoei, A. Oshnoei, A. Mosallanejad, F. Haghjoo, Contribution of GCSC to regulate the frequency in multi-area power systems considering time delays: A new control

outline based on fractional order controllers, International Journal of Electrical Power & Energy Systems 123 (2020) 106197. doi:10.1016/j.ijepes.2020.106197.

[6] H. A. Yousef, K. AL-Kharusi, M. H. Albadi, N. Hosseinzadeh, Load frequency control of a multi-area power system: An adaptive fuzzy logic approach, IEEE Transactions on Power Systems 29 (2014) 1822–1830. doi:10.1109/tpwrs.2013.2297432.

[7] T. Kerdphol, F. Rahman, Y. Mitani, K. Hongesombut, S. Küfeoğlu, Virtual inertia control-based model predictive control for microgrid frequency stabilization considering high renewable energy integration, Sustainability 9 (2017) 773. URL: https://doi.org/10.3390/su9050773. doi:10.3390/su9050773.

[8] K. Mentesidi, R. Garde, M. Aguado, E. Rikos, Implementation of a fuzzy logic controller for virtual inertia emulation, in: 2015 International Symposium on Smart Electric Distribution Systems and Technologies (EDST), IEEE, 2015. URL: https://doi.org/10.1109/sedst.2015.7315279. doi:10.1109/sedst.2015.7315279.

[9] Y. Ge, G. Liu, G. Zhao, H. Liu, J. Sun, Observer-based h∞ load frequency control for networked power systems with limited communications and probabilistic cyber attacks, Energies 15 (2022) 4234. URL: https://doi.org/10.3390/en15124234. doi:10.3390/en15124234.

[10] V. V. Huynh, B. L. N. Minh, E. N. Amaefule, A.-T. Tran, P. T. Tran, Highly robust observer sliding mode based frequency control for multi area power systems with renewable power plants, Electronics 10 (2021) 274. URL: https://doi.org/10.3390/electronics10030274. doi:10.3390/electronics10030274.

[11] R. A. Maher, I. A. Mohammed, I. K. Ibraheem, Polynomial based h∞ robust governor for load frequency control in steam turbine power systems, Interna-

tional Journal of Electrical Power &amp Energy Systems 57 (2014) 311–317. URL:
https://doi.org/10.1016/j.ijepes.2013.12.010.
doi:10.1016/j.ijepes.2013.12.010.

[12] M. Shouran, F. Anayi, M. Packianather, The bees algorithm tuned sliding mode control
for load frequency control in two-area power system, Energies 14 (2021) 5701. URL:
https://doi.org/10.3390/en14185701. doi:10.3390/en14185701.

[13] Z. Al-Hamouz, H. Al-Duwaish, A new load frequency variable structure con-
troller using genetic algorithms, Electric Power Systems Research 55 (2000)
1–6. URL: https://doi.org/10.1016/s0378-7796(99)00095-4.
doi:10.1016/s0378-
7796(99)00095-4.

[14] D. Yousri, T. S. Babu, A. Fathy, Recent methodology based harris hawks opti-
mizer for designing load frequency control incorporated in multi-interconnected renew-
able energy plants, Sustainable Energy, Grids and Networks 22 (2020) 100352. URL:
https://doi.org/10.1016/j.segan.2020.100352.
doi:10.1016/j.segan.2020.100352.

[15] D. Kler, V. Kumar, K. P. Rana, Optimal integral minus proportional deriva-
tive controller design by evolutionary algorithm for thermal-renewable energy-hybrid
power systems, IET Renewable Power Generation 13 (2019) 2000–2012. URL:
https://doi.org/10.1049/iet-rpg.2018.5745. doi:10.1049/iet-rpg.2018.5745.

[16] S. Abd-Elazim, E. Ali, Load frequency controller design via BAT al-
gorithm for nonlinear interconnected power system, International Jour-
nal of Electrical Power &amp Energy Systems 77 (2016) 166–177. URL:
https://doi.org/10.1016/j.ijepes.2015.11.029.
doi:10.1016/j.ijepes.2015.11.029.

[17] R. K. Sahu, S. Panda, U. K. Rout, D. K. Sahoo, Teaching learning based op-

timization algorithm for automatic generation control of power system using 2-
DOF PID controller, International Journal of Electrical Power &amp Energy Sys-
tems 77 (2016) 287–301. URL: https://doi.org/10.1016/j.ijepes.2015.11.082.
doi:10.1016/j.ijepes.2015.11.082.

[18] E. Ali, S. Abd-Elazim, BFOA based design of PID controller for two area load frequency
control with nonlinearities, International Journal of Electrical Power &amp Energy Sys-
tems 51 (2013) 224–231. URL: https://doi.org/10.1016/j.ijepes.2013.02.030.
doi:10.1016/j.ijepes.2013.02.030.

[19] D. Guha, P. K. Roy, S. Banerjee, Load frequency control of interconnected
power system using grey wolf optimization, Swarm and Evolutionary Compu-
tation 27 (2016) 97–115. URL: https://doi.org/10.1016/j.swevo.2015.10.004.
doi:10.1016/j.swevo.2015.10.004.

[20] S. P. Singh, T. Prakash, V. Singh, M. G. Babu, Analytic hierarchy
process based automatic generation control of multi-area interconnected power
system using jaya algorithm, Engineering Applications of Artificial Intelli-
gence 60 (2017) 35–44. URL: https://doi.org/10.1016/j.engappai.2017.01.008.
doi:10.1016/j.engappai.2017.01.008.

[21] A. Agwa, Equilibrium optimization algorithm for automatic generation control of inter-
connected power systems, PRZEGLAD ELEKTROTECHNICZNY 1 (2020)145–150.
URL: https://doi.org/10.15199/48.2020.09.30. doi:10.15199/48.2020.09.30.

[22] M. Khamies, G. Magdy, M. Ebeed, S. Kamel, A robust PID controller based
on linear quadratic gaussian approach for improving frequency stability of power
systems considering renewables, ISA Transactions 117 (2021) 118–138. URL:

https://doi.org/10.1016/j.isatra.2021.01.052.
doi:10.1016/j.isatra.2021.01.052.

[23] J. Sharma, Y. V. Hote, R. Prasad, PID controller design for interval load frequency control system with communication time delay, Control Engineering Practice 89 (2019) 154–168. doi:10.1016/j.conengprac.2019.05.016.

[24] M. Eid, M. Aly, E. A. Mohamed, A. Fathy, S. HEshmat, Analysis and design of frequency regulation controllers with considering communication delays and environmental effects of renewable energy microgrids, Aswan University Journal of Environmental Studies 5 (2024)262–294. URL: http://dx.doi.org/10.21608/aujes.2024.287639.1235. doi:10.21608/aujes.2024.287639.123

[25] D. Yousri, T. S. Babu, A. Fathy, Recent methodology based harris hawks optimizer for designing load frequency control incorporated in multi-interconnected renewable energy plants, Sustainable Energy, Grids and Networks 22 (2020) 100352. doi:10.1016/j.segan.2020.100352.

[26] D. K. Gupta, A. K. Soni, A. V. Jha, S. K. Mishra, B. Appasani, A. Srinivasulu, N. Bizon, P. Thounthong, Hybrid gravitational–firefly algorithm-based load frequency control for hydrothermal two-area system, Mathematics 9 (2021) 712. URL: https://doi.org/10.3390/math9070712. doi:10.3390/math9070712.

[27] N. Mishra, S. K. Jena, P. K. Behera, B. K. Sahu, Proper selection of different parameters of DE algorithm to study the dynamic performance of AGC in a two area hydrothermal system, in: 2014 International Conference on Advances in Electrical Engineering (ICAEE), IEEE, 2014. URL: https://doi.org/10.1109/icaee.2014.6838523. doi:10.1109/icaee.2014.6838523.

[28] H. Rezk, M. A. Mohamed, A. A. Zaki Diab, N. Kanagaraj, Load frequency control of multi interconnected renewable energy plants using multi-verse optimizer,

Computer Systems Science and Engineering 37 (2021) 219–231. URL:http://dx.doi.org/10.32604/csse.2021.015543. doi:10.32604/csse.2021.015543

[29] E. M. Ahmed, M. Aly, A. Elmelegi, A. G. Alharbi, Z. M. Ali, Multi-functional distributed MPPT controller for 3p4w grid-connected PV systems in distribution network with unbalanced loads, Energies 12 (2019) 4799. URL: https://doi.org/10.3390/en12244799. doi:10.3390/en12244799.

[30] A. Elmelegi, M. Aly, E. M. Ahmed, A. G. Alharbi, A simplified phase-shift PWM-based feedforward distributed MPPT method for grid-connected cascaded PV inverters, Solar Energy 187 (2019) 1–12. URL: https://doi.org/10.1016/j.solener.2019.05.021. doi:10.1016/j.solener.2019.05.021.

[31] E. M. Ahmed, A. Elmelegi, A. Shawky, M. Aly, W. Alhosaini, E. A. Mohamed, Frequency regulation of electric vehicle-penetrated power system using MPA-tuned new combined fractional order controllers, IEEE Access 9 (2021) 107548–107565. URL: https://doi.org/10.1109/access.2021.3100800. doi:10.1109/access.2021.3100800.

[32] E. M. Ahmed, E. A. Mohamed, A. Elmelegi, M. Aly, O. Elbaksawi, Optimum modified fractional order controller for future electric vehicles and renewable energy-based interconnected power systems, IEEE Access 9 (2021) 29993–30010. URL: https://doi.org/10.1109/access.2021.3058521. doi:10.1109/access.2021.3058521.

[33] A. Faramarzi, M. Heidarinejad, S. Mirjalili, A. H. Gandomi, Marine predators algorithm: A nature-inspired metaheuristic, Expert Systems with Applications 152 (2020) 113377. URL: http://dx.doi.org/10.1016/j.eswa.2020.113377. doi:10.1016/j.eswa.2020.113377.

[34] M. Aly, E. M. Ahmed, H. Rezk, E. A. Mohamed, Marine predators algo-
rithm optimized reduced sensor fuzzy-logic based maximum power point tracking
of fuel cell-battery standalone applications, IEEE Access 9 (2021) 27987–28000.
doi:10.1109/access.2021.3058610.